Proceedings of the ASME 2021 16th International Manufacturing Science and Engineering Conference
MSEC2021
June 21-25, 2021, Cincinnati, OH, USA

MSEC2021-59877

NUMERICAL ANALYSIS OF SS316L BIAXIAL CRUCIFORM SPECIMENS UNDER PROPORTIONAL LOADING PATHS

Elizabeth M. Mamros, Matthew C. Eaton, Jinjin Ha, Brad L. Kinsey

Department of Mechanical Engineering
University of New Hampshire
Durham, NH, USA

ABSTRACT

In this paper, finite element analyses were conducted to investigate the stress and strain states resulting from varying the deformation of stainless steel 316L under biaxial loading. To that end, a biaxial specimen geometry was designed in collaboration with the US National Institute of Standards and Technology (NIST) to achieve large and uniform strain values in the central pocket region. Special care was taken to ensure that the specimen design could be readily manufactured with available resources. Simultaneously, the specimen design criteria required an acceptable strain uniformity in a sufficiently large pocket section to allow for accurate deformation and austenite to martensite phase fraction measurements. This demonstrates the concept of altering the final material properties through stress superposition. Numerical results show that nearly linear curves were observed in the strain path plots. The minimum uniform deformation area for the 4:1 case had a radius of ~1 mm, which is sufficient for experimental analyses, e.g., digital imaging correlation and electron beam backscatter diffraction. As an application for such heterogeneous materials, patient specific trauma fixation hardware, which are surgically implanted to set broken bones during healing, require high strength in areas where screws are located, i.e., martensite phase, yet low weight elsewhere.

Keywords: cruciform, in-plane biaxial, finite element, stainless steel

1. INTRODUCTION

To fully characterize material plastic anisotropy, data collection from several different types of experiments is required to calibrate the yield function, which is essential for modeling the complex forming operations in manufacturing. In addition to uniaxial tensile tests, experiments are often conducted on custom biaxial loading frames, e.g., [1] at the University of New Hampshire (UNH), to probe in-plane biaxial deformation modes. In the past three decades, dozens of studies have investigated potential cruciform specimen geometry designs, often building on the work of Kuwabara et al. [2], which established ISO standard 16842 [3], yet an ASTM standard has not been established. Often, these designs share common objectives: strain uniformity, minimal shear strains, and failure in the gauge section; decreased stress concentrations elsewhere; and repeatable results [4]. One common limitation of cruciform geometries is that failure occurs at relatively low plastic strain values, which are typically <15%. To better capture the material behavior, it is desired to have a specimen that can be deformed over a larger plastic strain range.

Another complication with biaxial specimen designs is that expensive machining operations are often required to create intricate features. For example, wire electrical discharge machining (EDM) or laser cutting is necessary to create relief slits or slots in the specimen arms to address the issue of premature failure in these regions. Another potential solution is to reinforce the thickness of the material surrounding the gauge section so that the deformation can be concentrated in the center cross-sectional area. Zhao et al. [5] created a thickness-increased, sandwich specimen that incorporates the use of metallic pieces and achieves approximately 15% equivalent plastic strain in the center. As an alternative strategy, Hou et al. [6] increased the material thickness in the specimen arms with the addition of material from laser deposition.

As opposed to thickness reinforcement, thickness reduction is also an effective approach to achieve large strain values for the cruciform type specimen. Instead of a typical square-shaped reduced thickness area in the gauge section [7], the National Institute of Standards and Technology (NIST) [8] and other

researchers [8, 9] have experimented with designs involving circular pockets with a prescribed fillet radius to prevent a sharp corner at the thickness transition into the gauge area. With these complex cross-sectional areas, inverse finite element analyses (FEA) are required to determine the stress state corresponding to experimental results.

One major benefit of the biaxial cruciform specimen is that the deformation paths can be intentionally controlled via stress superposition to tailor the material properties of the deformed metal to the desired application. Loading the specimen proportionally results in complex, biaxial stress states. Changing the loading conditions during the deformation, e.g., initially loading equibiaxially and then switching to plane-strain loading state at a specified displacement, will result in even more complex, superimposed stress states with increased opportunities for manipulation. This flexibility is critical for creating customized components, e.g., patient-specific trauma hardware, through controlled austenite to martensite transformation in stainless steels.

In this paper, FEA of a cruciform specimen geometry, created in collaboration with NIST, are presented for six different loading cases ranging approximately from uniaxial to equibiaxial tension. With the intent that the data collected from this specimen will determine stress superposition deformation paths when forming trauma fixation hardware, which is the application of interest, the material selected was 1.2 mm thick sheets of biocompatible stainless steel (SS) 316L, which exhibits a stress-assisted, microstructural phase change from austenite to martensite. This specimen geometry achieved all design specifications including linear strain paths, a gauge section large enough for measurements during and after experiments, and machinable dimensions. Future experiments will quantify the limitations of this geometry and validate the numerical results.

2. Methodology

The methodology for this work includes the material and specimen geometry of interest in addition to the numerical analyses conducted using a finite element model.

2.1 Material and Specimen Geometry

As part of a collaboration with NIST, a biaxial specimen geometry was designed to increase the maximum achievable plastic strain in the circular pocket area as compared to previous specimen designs. Other design criteria included a specimen that maintains linear strain paths, a pocket area sufficiently large for state-of-the-art characterization techniques, and machinable dimensions. A coupled numerical analysis and specimen fabrication approach was utilized to determine the specimen geometry and dimensions using a sheet thickness of 1.2 mm as shown in Fig. 1.

The pocket area is a reduced thickness section (half of the material thickness = 0.6 mm) in the center of the specimen that consists of a flat 9.01 mm diameter area connected to the specimen surface at the sheet thickness by a 1.02 mm fillet radius. This flat area is of interest for digital image correlation (DIC) and infrared imaging *in situ* for strain and temperature measurements, respectively. This region also meets the size requirements for post analyses such as electron backscatter diffraction (EBSD) or measurement using a ferritescope to determine the volume fraction of martensite. The specimen is symmetrical about all three planes. In each of the four notches surrounding the pocket area, a 2.48 mm radius is used to connect the perpendicular arms to reduce stress concentrations in these areas.

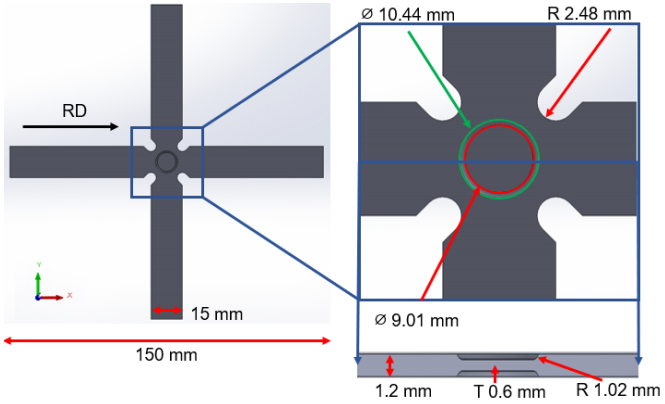

FIGURE 1: BIAXIAL CRUCIFORM SPECIMEN GEOMETRY

While not physically tested yet, specimens have been fabricated for future cruciform testing. The specimen outline was waterjet cut, with the arms oriented along the rolling and transverse directions, followed by a milling operation. The toolpath for the milling involved circular interpolation since the tool diameter (1.02 mm) is much smaller than the pocket size followed by a finishing pass on both sides of the specimen. Lastly, polishing in the milled pocket was performed using diamond compounds to achieve the desired surface finish. The specimen dimensions were measured with a confocal microscope (Olympus OLS5000-SAF) to confirm that all dimensions were within the desired tolerance, i.e., ±2%.

Hockett-Sherby isotropic hardening law (Eq. 1) was fit to data from a uniaxial tension experiment in the rolling direction (RD) using the parameters in Table 1 and extrapolated as shown in Fig. 2.

$$\bar{\sigma} = \sigma_\infty - \exp\left(-n \cdot \bar{\varepsilon}_{pl}{}^{p}\right) \cdot (\sigma_\infty - \sigma_y) \qquad (1)$$

TABLE 1. STRAIN HARDENING PARAMETERS FOR HOCKETT-SHERBY HARDENING LAW FOR SS316L

σ_∞ [MPa]	σ_y [MPa]	n	p
1445.44	339.48	1.81	0.89

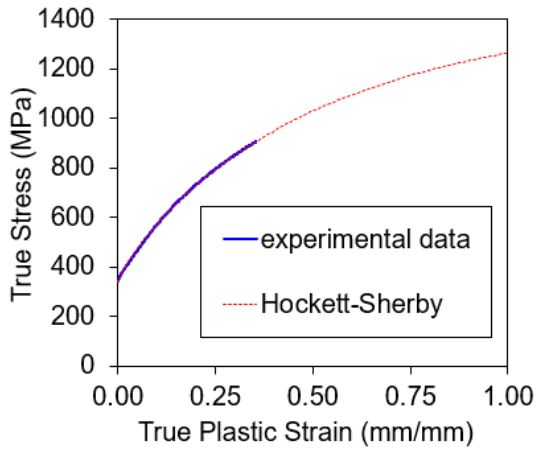

FIGURE 2: HOCKETT-SHERBY FIT TO SS316L TRUE STRESS-STRAIN CURVE FROM UNIAXIAL TENSION IN THE RD EXPERIMENT

2.2 Simulation Outline

A finite element model was constructed in ABAQUS 2019 [11] using the implicit solver with isotropic elasticity and von Mises yield function combined with isotropic strain hardening for plasticity. Due to symmetry, a one-eighth model of the biaxial cruciform specimen was created and meshed with approximately 75,000 C3D8R elements. A slightly shortened arm length compared to the specimen design was used to decrease computational expense after confirming that this dimension reduction would not impact the results. There are six elements through the half-thickness, and the mesh is finest in the pocket region as shown in Fig. 3.

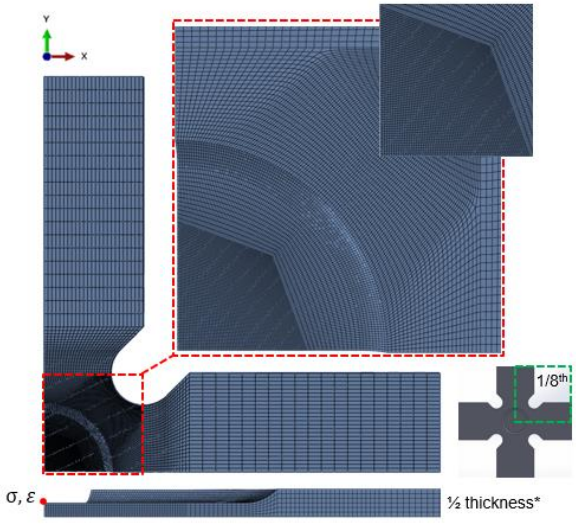

FIGURE 3: MESHED, 1/8TH MODEL OF CRUCIFORM SPECIMEN WITH ~75K ELEMENTS [NOTE: THICKNESS IS NOT TO SCALE.]

To vary the deformation paths, displacement boundary conditions were applied to the perpendicular surface of each specimen arm with the following ΔY: ΔX displacement (in mm) ratios: 4: 4 (close to equibiaxial tension), 4: 3, 4: 2, 4: 1, 4: 0, and 4:free (close to uniaxial). A terminating failure criterion was not implemented for these simulations.

3. Results and Discussion

To determine if the specimen design criteria were achieved with this geometry, stress and strain path plots as well as stress and strain contour plots were extracted from the simulations. Additionally, fabricated specimens were measured using the confocal microscope to assess the dimensions of the pocket for machinability.

The true stress and strain paths for each of the six loading cases studied in this work are shown in Fig. 4. Both are extracted at the center, surface node of the specimen, equivalent to the center of the pocket, marked with a red dot in Fig. 3. In the stress path plot, a transition point is visible for all cases except for equibiaxial as σ_{yy} approaches the initial yield strength (~340 MPa) of the material. In other words, this transition point is indicative of the transition from elastic to plastic deformation, which is not smooth due to the non-uniform transition in the pocket region. The elastic region, i.e., when PEEQ = 0, is shown with a dashed line, and the plastic region, i.e., when PEEQ is non-zero, is represented by a solid line in Fig. 4a. At strains $\varepsilon_{yy} <$ 3%, the strain paths appear slightly non-linear. At larger strain values, the strain paths have minimal non-linearity, with the 4:2 case exhibiting the largest deviation from linearity. Since a failure criterion was not implemented in these simulations, experiments are needed to determine the maximum achievable strains with this specimen geometry. These reasonably linear strain paths and predicted principle strain values are encouraging that this specimen geometry will provide measurable, strain-assisted martensite transformation for the given deformation paths.

To ensure accurate measurements of the martensite volume fractions in experiments, high strain uniformity is desired in the pocket region. The equivalent plastic strain (PEEQ) values were extracted from every surface node within the pocket for all frames and compared against the value from the central node. Similarly, PEEQ was probed at the midplane, which yielded comparable results and thus are not presented here. Examples of the strain contour plots can be seen in Fig. 5 for the (a) 4:4 equibiaxial and (b) 4:1 displacement cases from the simulation frame where the maximum PEEQ = 0.6 in the notch. For measurement purposes, PEEQ values within 2.5% of the central node value are considered sufficiently uniform. Thus, at the selected frame, the uniformity is evaluated by the minimum radius of the red zone from the specimen center in Fig. 5, and it is approximately 2.75 mm for the 4:4 case and 0.92 mm for the 1:1 case. A sample size of approximately 1 mm^2 is recommended for EBSD measurements; therefore, a sample with minimal non-uniformity could be extracted from the center of the pocket region of this specimen geometry. The ferritescope (Fischer Technology) probe specifies a 3 mm radius for minimal error, so physical experiments are required to determine the amount of potential error for this measurement method for certain displacement cases (e.g., 4:1).

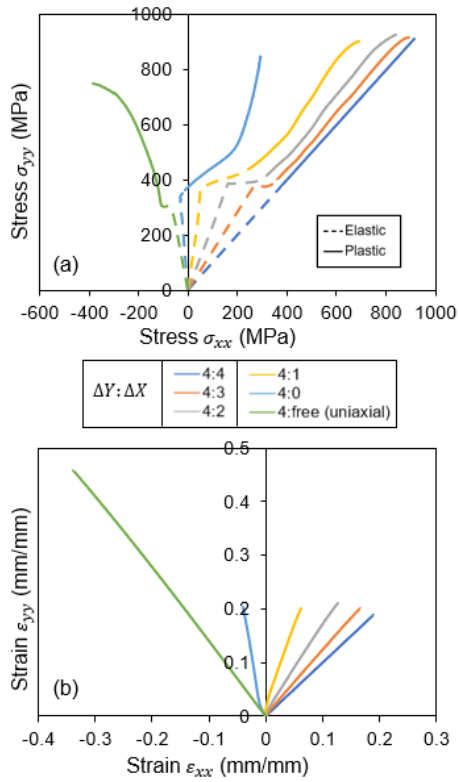

FIGURE 4: SIMULATED TRUE (A) STRESS AND (B) LOGARITHMIC STRAIN PATHS, EXTRACTED FROM THE CENTER OF THE POCKET, FOR EACH $\Delta Y:\Delta X$ DISPLACEMENT CASE

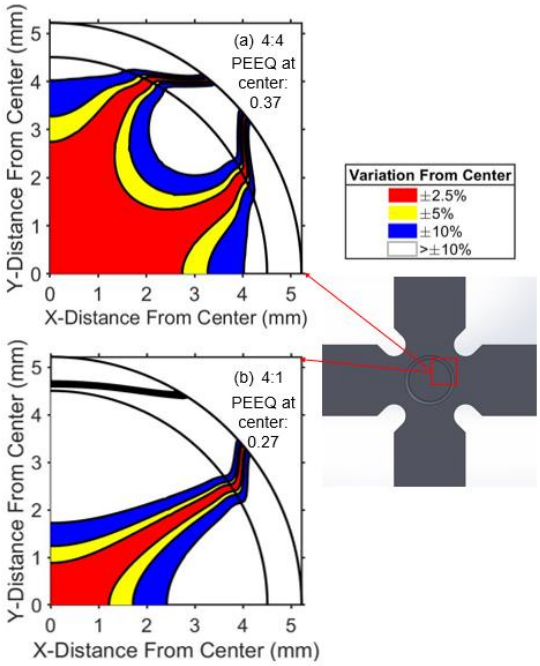

FIGURE 5: EQUIVALENT PLASTIC STRAIN (PEEQ) CONTOURS FOR (a) 4:4 AND (b) 4:1 DISPLACEMENTCASES IN THE POCKET AREA WITH REFERENCE TO THE CENTER SURFACE NODE

For all displacement cases, a stress concentration developed in the specimen notches as the plastic strain level increased. Figure 6a shows an example for the 4:4 displacement case, with approximately 1080 MPa von Mises equivalent stress appearing in the notch when the PEEQ at the center of the specimen is approximately 0.37. A similar stress concentration plot for the 4:1 displacement case is shown in Fig. 6b. As the simulation progressed, the stress concentrations in the notches elongated and eventually connected to the stress concentrations shown in the pocket region. The corresponding equivalent plastic strain contours (PEEQ) are shown in Fig. 7.

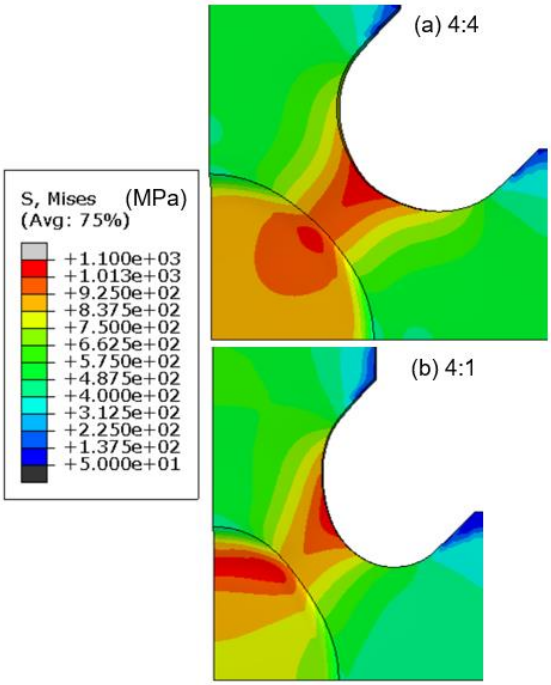

FIGURE 6: STRESS CONCENTRATIONS IN SPECIMEN NOTCHES FOR (a) 4:4 AND (b) 4:1 DISPLACEMENT CASES

Since a terminating criterion was not utilized in the simulations, experiments are needed to determine if the specimen will fail due to crack propagation outward from the pocket region or due to the stress concentration first observed in the notch. Similar biaxial geometries tested experimentally have shown a propensity towards failure in the notched region prior to the gauge area [7]. Since fracture characterization is not an objective for this cruciform specimen, it is recommended that alternative specimen geometries be used to study the fracture behavior of the material.

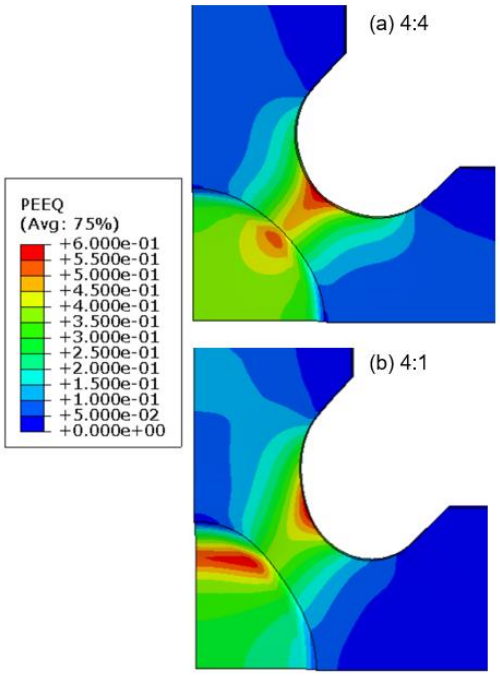

FIGURE 7: EQUIVALENT PLASTIC STRAIN (PEEQ) FOR (a) 4:4 AND (b) 4:1 DISPLACEMENT CASES

After milling the specimen pocket but prior to polishing, cruciform specimens were measured using the confocal microscope to verify the critical dimensions identified in Fig. 1. Figure 8 presents a topography analysis conducted across the specimen pocket area. The diameter of the flat region (9.06 mm) and depth of the pocket (307 µm average) were also measured from this analysis by determining the absolute differences between the appropriate extrema. Thickness variation exists across the pocket region from the milling operation with a maximum variation of ~10 µm, i.e., ~3% of the pocket half-thickness (0.3 mm), as shown in the figure inset. However, after polishing with diamond compound, this value falls within the specified tolerance. Thus, the machinability of this specimen design using the previously described methodology was validated.

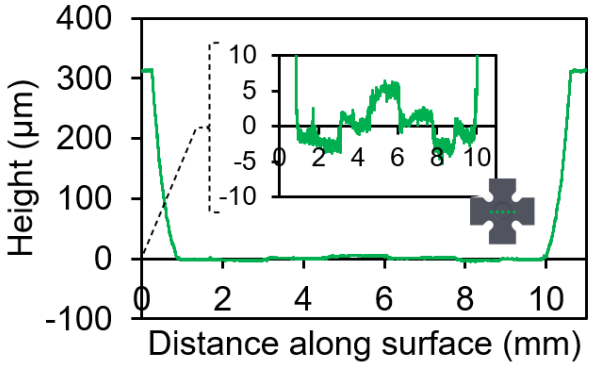

FIGURE 8: CONFOCAL MICROSCOPE TOPOGRAPHY PLOT ACROSS CRUCIFORM SPECIMEN CENTERLINE

4. CONCLUSIONS AND OUTLOOK

A preliminary, machinable cruciform specimen design was created in collaboration with NIST that will be optimized further. Finite element models predict that the specimen geometry will meet the desired objectives specified of large, uniform strain distribution in the pocket region. Nearly linear strain paths were observed in the strain path plots. The minimum uniform deformation area for the 4:1 case had a radius of ~1 mm, which is sufficient for DIC and EBSD analyses.

Future work will include the measurement of martensite transformations and constitutive modeling for the numerical simulations to allow volume fraction predictions. These values will be utilized to determine the stress superposition deformation paths for a rapid prototyping, incremental forming machine to produce custom, biocompatible components with the desired final heterogeneous part properties. Additionally, experiments will be conducted to validate all numerical results and quantify limitations of this specimen geometry, e.g., maximum achievable displacement prior to fracture for a given loading case.

ACKNOWLEDGEMENTS

The authors would like to thank Mark Iadicola and Dilip Banerjee from the US NIST for their assistance in obtaining a feasible geometry and their support during this collaboration. The Olympus confocal microscope used is managed by the University Instrumentation Center (UIC) at the University of New Hampshire (UNH). This research is supported by US National Science Foundation EPSCoR award (#1757371).

REFERENCES

[1] Wilson, J. F., Kinsey, B. L., and Korkolis, Y. P., 2013, "Development of a Biaxial Loading Frame for Sheet Metal," J. Manuf. Process., **15**(4), pp. 580–585.

[2] Kuwabara, T., Ikeda, S., and Kuroda, K., 1998, "Measurement and Analysis of Differential Work Hardening in Cold-Rolled Steel Sheet under Biaxial Tension," J. Mater. Process. Technol., **80–81**, pp. 517–523.

[3] International Organization for Standardization, 2014, "Metallic Materials — Sheet and Strip — Biaxial Tensile Testing Method Using a Cruciform Test Piece (ISO 16842)," ISO.

[4] Banerjee, D. K., Iadicola, M. A., Creuziger, A. A., and Foecke, T. J., 2015, "An Experimental and Numerical Study of Deformation Behavior of Steels in Biaxial Tensile Tests."

[5] Zhao, K., Chen, L., Xiao, R., Ding, Z., and Zhou, L., 2019, "Design of a Biaxial Tensile Testing Device and Cruciform Specimens for Large Plastic Deformation in the Central Zone," J. Mater. Sci., **54**(9), pp. 7231–7245.

[6] Hou, Y., Min, J., Lin, J., Carsley, J. E., and Stoughton, T. B., 2018, "Cruciform Specimen Design for Large Plastic Strain during Biaxial Tensile Testing," J. Phys. Conf. Ser., **1063**, p. 012160.

[7] Deng, N., Kuwabara, T., and Korkolis, Y. P., 2015, "Cruciform Specimen Design and Verification for Constitutive Identification of Anisotropic Sheets," Exp. Mech., **55**(6), pp. 1005–1022.

[8] Iadicola, M. A., Creuziger, A. A., and Foecke, T., 2014, "Advanced Biaxial Cruciform Testing at the NIST Center for Automotive Lightweighting," *Residual Stress, Thermomechanics & Infrared Imaging, Hybrid Techniques and Inverse Problems, Volume 8*, M. Rossi, M. Sasso, N. Connesson, R. Singh, A. DeWald, D. Backman, and P. Gloeckner, eds., Springer International Publishing, Cham, pp. 277–285.

[9] Abu-Farha, F., Hector, L. G., and Khraisheh, M., 2009, "Cruciform-Shaped Specimens for Elevated Temperature Biaxial Testing of Lightweight Materials," JOM, **61**(8), pp. 48–56.

[10] Upadhyay, M. V., Patra, A., Wen, W., Panzner, T., Van Petegem, S., Tomé, C. N., Lebensohn, R. A., and Van Swygenhoven, H., 2018, "Mechanical Response of Stainless Steel Subjected to Biaxial Load Path Changes: Cruciform Experiments and Multi-Scale Modeling," Int. J. Plast., **108**, pp. 144–168.

[11] 2019, *ABAQUS*, Dassault Systèmes Simulia Corporation, Providence, RI, USA.